

Reactive Sputtering of Bismuth Vanadate Photoanodes for Solar Water Splitting

Le Chen,^{†,‡} Esther Alarcón-Lladó,^{†,‡,||} Mark Hettick,^{†,‡,⊥} Ian D. Sharp,^{†,§} Yongjing Lin,^{†,‡,⊥} Ali Javey,^{†,‡,⊥} and Joel W. Ager^{*,†,‡}

[†]Joint Center for Artificial Photosynthesis, Lawrence Berkeley National Laboratory, Berkeley, California 94720, United States

[‡]Materials Sciences Division, Lawrence Berkeley National Laboratory, Berkeley, California 94720, United States

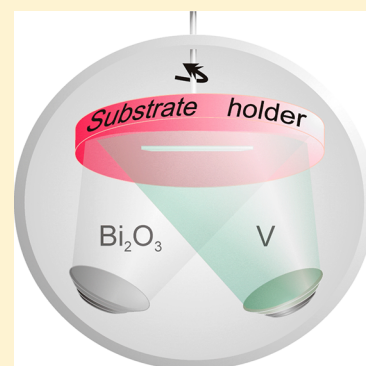
[§]Physical Biosciences Division, Lawrence Berkeley National Laboratory, Berkeley, California 94720, United States

^{||}École Polytechnique Fédérale de Lausanne, Lausanne, Switzerland

[⊥]Department of Electrical Engineering and Computer Sciences, University of California, Berkeley, Berkeley, California 94720, United States

Supporting Information

ABSTRACT: Bismuth vanadate (BiVO_4) has attracted increasing attention as a photoanode for photoelectrochemical (PEC) water splitting. It has a band gap in the visible light range (2.4–2.5 eV) and a valence band position suitable for driving water oxidation under illumination. While a number of methods have been used to make BiVO_4 photoanodes, scalable thin film deposition has remained relatively underexplored. Here, we report the synthesis of BiVO_4 thin films by reactive sputtering. The use of separate Bi and V sputtering targets allows control of the Bi/V ratio in the film. Under optimized, slightly V-rich conditions, monoclinic phase BiVO_4 with photoactivity for water oxidation is obtained. The highest photocurrents, ca. 1 mA cm^{-2} at the reversible $\text{O}_2/\text{H}_2\text{O}$ potential with simulated AM 1.5G illumination, are obtained with bilayer $\text{WO}_3/\text{BiVO}_4$, where the WO_3 serves as a hole-blocking layer.



I. INTRODUCTION

Bismuth vanadate (BiVO_4) has been studied since the late 1990s as a water oxidation photocatalyst^{1,2} and also as an alternative photocatalyst to TiO_2 for organic pollutant removal.^{3,4} Recently, there has been growing interest in using BiVO_4 as a photoanode for photoelectrochemical water splitting.^{5,6} BiVO_4 has a number of attractive material properties for this purpose. It has a band gap in the visible region of the electromagnetic spectrum, 2.4–2.5 eV, is composed of abundant and nontoxic elements, and has been reported to drive water oxidation with an onset potential of up to 0.3 V vs RHE (0.9 V vs the reversible $\text{O}_2/\text{H}_2\text{O}$ potential),^{7,8} which makes it attractive for pairing with hydrogen-producing photocathodes in a tandem water splitting arrangement.^{6,9}

Park et al. have recently reviewed the current status of BiVO_4 photoanodes.⁶ For use in tandem water splitting geometry, it must be possible to electrically contact the BiVO_4 in either a thin film or equivalent nanostructured configuration. The most widely used synthesis methods use solution phase chemistry coupled with spin-coating or spray pyrolysis to make BiVO_4 films.^{10–14} Electrochemical deposition has also been reported.^{6,15,16} For unmodified BiVO_4 , reported photocurrents for water oxidation with AM1.5 illumination are lower than 1 mA cm^{-2} ,^{7,16–18} which is less than 15% of the theoretical maximum for a 2.4 eV absorber (7.5 mA/cm^2). Known issues with BiVO_4 include poor electron transport, as evidenced by

higher photocurrents for back as opposed to front illumination and slow water oxidation kinetics.^{15,19} Doping, cocatalysts such as Co-Pi and hole-blocking back contacts have been found to improve performance significantly.^{13,14,20}

Physical vapor deposition (PVD) methods for the synthesis of BiVO_4 have been explored relatively little.^{17,21} Sputtering is a commercially available and scalable physical vapor deposition process which has been used to make a number of metal oxide or nitride thin film materials such as TiO_2 , WO_3 , and TaON for photocatalytic and photoelectrochemical applications.^{22–24} Some potential advantages of sputter deposition are control of stoichiometry, film uniformity and adhesion, and ability to make a dense film for the evaluation of fundamental properties. In this study, we report the synthesis of high quality BiVO_4 thin films for PEC application by reactive sputtering. Bi and V have very different sputtering yields, so separate Bi and V precursor targets were used to produce the desired phase of BiVO_4 and control over the Bi/V ratio. We find that a slight V excess yields the best water oxidation performance, which can be further improved by hole-blocking back contact.^{18,19}

Received: June 18, 2013

Revised: September 20, 2013

Published: September 23, 2013

II. EXPERIMENTAL METHODS

Synthesis. All depositions were performed with an AJA International ATC Orion 5 sputtering machine equipped with a load lock. Use of a single BiVO₄ target was not successful in producing stoichiometric BiVO₄ films as Bi was preferentially depleted from the target. Instead, we used a cosputtering approach using separate two inch diameter bismuth oxide (Bi₂O₃, 99.9%) and vanadium (V, 99.99%) targets, as shown in Figure 1. Because of the large thermal conductivity disparity

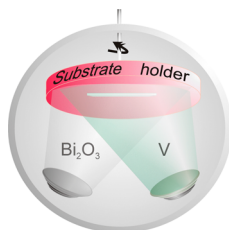


Figure 1. Illustration of the cosputtering of Bi₂O₃ and V to deposit BiVO₄ thin films.

between Bi₂O₃ (0.7–0.9 W·m⁻¹·K⁻¹) and V (30.7 W·m⁻¹·K⁻¹),²⁵ two different target power supplies were used to independently tune the Bi and V sputtering rates. We found that the combination of a high-power direct current (dc) power supply for the vanadium target source and a radio frequency (rf) power supply for the bismuth oxide target yielded the greatest degree of compositional control. Typical operation power range was 35–40 W for the Bi₂O₃ rf power supply and 180–185 W for the V dc power supply.

A mixture of Ar and O₂ was used for reactive sputtering. We found that the O₂ partial pressure affected the sputtering yield, especially for the V target. Lower O₂ partial pressures increased the sputtering yields for vanadium. Following optimization, we selected a total pressure of 5.1 mTorr, with partial pressures of 4.5 mTorr Ar and 0.6 mTorr O₂, for all films reported in this work. These conditions resulted in a deposition rate of approximately 2.5 nm/min. The indium doped tin oxide (ITO) coated glass substrates were held at room temperature during deposition, and the resulting films were annealed in a tube furnace under air at 500 °C for 2 h.

Characterization and Measurement. The morphology and bulk elemental composition (Bi to V atomic ratio) of the films were characterized using an FEI Quanta 200 FEG scanning electron microscope (SEM) with a Bruker Quantax energy dispersive spectroscopy (EDS) attachment. Film thickness was measured using a DEKTAk IA profilometer (Veeco) to determine the step height at a masked edge. Bulk crystalline structure of the films was characterized using a Rigaku Smartlab X-ray diffractometer. Phase assignments were made based on the Joint Committee on Powder Diffraction Standards (JCPDS) database. Additional structural characterization was achieved via Raman spectroscopy using a Horiba Yvon Jobin LabRAM HR confocal Raman microscope with a laser excitation wavelength of 633 nm and power of 0.1–0.3 mW at the objective (spot size of approximately 1 μm). The optical absorbance spectrum was measured by a Shimadzu SolidSpec-3700 UV–vis-NIR Spectrophotometer.

Surface elemental analysis was carried out by X-ray photoelectron spectroscopy (XPS) using a monochromatized Al Kα source ($h\nu = 1486.6$ eV), operated at 225 W, on a Kratos Axis Ultra DLD system at a takeoff angle of 0° relative to the

surface normal. A pass energy of 20 eV, corresponding to an instrument resolution of approximately 600 meV, was used for narrow scan spectra. Survey spectra were collected with a pass energy of 80 eV. Spectral fitting was achieved using Casa XPS analysis software. Core level positions were calibrated to the primary C 1s core level position of 284.8 eV, and curves were fit with quasi-Voigt lines following Shirley background subtraction.

Photoelectrochemical (PEC) characterization was carried out using a BioLogic SP-300 potentiostat, in a three-electrode configuration, with a BASi RESB Ag/AgCl reference electrode, platinum mesh counter electrode, and the sputtered BiVO₄ films as the working electrode, in a quartz-windowed cell. The illumination source for *J–V* characterization was a Solar Light 16S-300–005 solar simulator equipped with an AM1.5 filter set. The light intensity of 100 mW/cm² was adjusted and calibrated using a Solar Light PMA-2100 radiometer and a PMA-2144 pyranometer. The electrolyte used for all measurements was 0.5 M Na₂SO₄ in 0.1 M K₂HPO₄ buffer solution (pH 7).

Spectrally resolved photocurrents for incident photon to charge conversion efficiency (IPCE) determination were generated using a Newport 150W Xe lamp and an Oriel Cornerstone 1/8m monochromator with 1.5 mm slits, yielding a spectral resolution of better than 0.5 nm. A beam splitter, together with a Thorlabs FDS1010-CAL calibrated Si photodiode, was used to monitor the intensity of the monochromatic output during the measurement. In order to ensure accurate measurement, the incident light spot under-filled both the sample and reference diode. A Gamry Reference 600 potentiostat was used in combination with a three-electrode electrochemical cell to maintain the sample at the reported potentials and to measure the current of the photoanode. The IPCE was then calculated based on the following formula:^{14,26}

$$\text{IPCE (\%)} = \frac{1240 \times j_{\text{ph}} \left(\frac{\text{mA}}{\text{cm}^2} \right)}{I_{\text{incident}} \left(\frac{\text{mW}}{\text{cm}^2} \right) \times \lambda (\text{nm})} \times 100\%$$

where j_{ph} is the measured photocurrent density in mA/cm², I_{incident} is the incident light intensity in mW/cm², and λ is the incident photon wavelength in nm.

III. RESULTS/DISCUSSION

Since near-stoichiometric films of BiVO₄ possess optical and electronic properties that are desirable for photoelectrochemical water splitting, we primarily explored Bi to V ratios within the compositional range of 40/60 to 60/40, with a goal of forming monoclinic BiVO₄ as the main product. In the following discussion, we will concentrate on the properties of three representative films with Bi/V ratios of approximately 61/39, 42/58, and 49.2/50.8, as determined by EDS. For each sample, we selected multiple points at different regions of the sample for EDS measurement, and the measured Bi to V ratios were consistent to within the range of experimental error, indicating that the films are compositionally uniform. These three films with different Bi to V ratios will be referred to as Bi-rich, V-rich, and stoichiometric for the remainder of this article. However, we note that the stoichiometric BiVO₄ film contains a slight excess of V, which will be discussed in greater detail below. Unless otherwise noted, all samples are approximately 100 nm thick.

Scanning electron microscopy (SEM) was used to determine the morphologies of the sputtered thin films as a function of composition. As shown in Figure 2, all films displayed grains

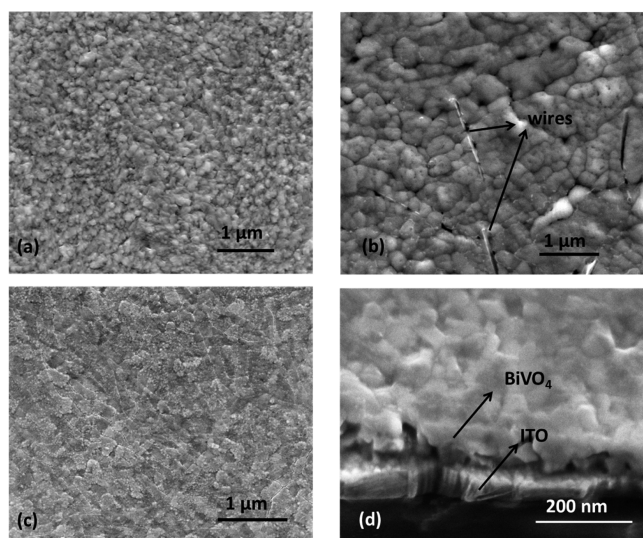


Figure 2. SEM images of reactively sputtered bismuth vanadium oxide thin films with Bi-rich (a), V-rich (b), and stoichiometric (BiVO_4) (c) compositions. (d) Thirty degree tilt view image of c.

indicative of polycrystalline structures. The stoichiometric film (Figure 2c) was characterized by smooth and distinctive grains of a few hundred nanometers in size, whereas the Bi-rich film (Figure 2a) exhibited a rougher surface with less distinctive grain boundaries. The V-rich film also displayed a polycrystalline structure; however, the size of the grains was much bigger but not as uniform as that for the two other samples. Furthermore, some wire-like structures, which resemble the morphology of V_2O_5 , were observed. Indeed, additional characterization, discussed below, confirmed the presence of the V_2O_5 impurity phase in these films. Figure 2d shows the cross-section image of the stoichiometric BiVO_4 film. As indicated in the figure, the film thickness is about 100 nm, and the film is continuous and dense.

Figure 3 shows XRD spectra from the Bi-rich, V-rich, and stoichiometric films deposited on ITO-coated glass. Since the films are thin (100 nm), peaks from the ITO substrate were also observed, as indicated by X's in the figure. The primary crystal structure of all 3 films is the monoclinic scheelite phase (vertical dashed lines), which is the most active BiVO_4 phase for photocatalysis or photoelectrochemical water split-

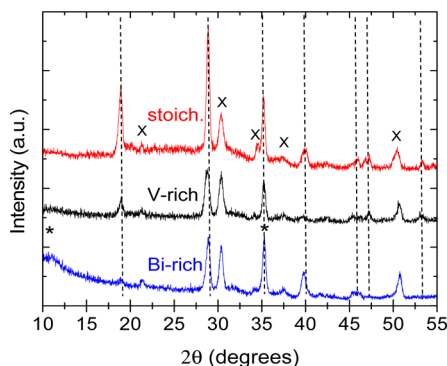


Figure 3. X-ray diffractograms of the Bi-rich (blue), V-rich (black), and stoichiometric (red) sputtered films. The X labeled peaks are from the ITO substrate, and the vertical dashed lines indicate the peaks from the monoclinic BiVO_4 structure. The "*" labeled peaks could arise or include contributions from $\text{Bi}_2\text{VO}_{5.5}$.

ting.^{10,27,28} For the Bi-rich film, in addition to the pattern of the BiVO_4 monoclinic structure, a weak and broad peak appears near 2θ values of $11\text{--}12^\circ$. This can be assigned to the $\text{Bi}_2\text{VO}_{5.5}$ (002) reflection, showing that excess Bi can produce phase segregation in the film. We also suspect that the peak at a 2θ value of 35° may include combined contributions from the BiVO_4 (002) and $\text{Bi}_2\text{VO}_{5.5}$ (006) reflections. For the V-rich film, we do not observe evidence of phase segregation (e.g., formation of crystalline V_2O_5) in XRD, but we do using Raman spectroscopy, as discussed below. In both the off-stoichiometric films, the dominant BiVO_4 (121) peak near 28° is shifted slightly to a lower diffraction angle, indicating an increase of the lattice constant due to the addition of excess Bi or V. We also note that there is a relative peak intensity reduction for some of the minor peaks (e.g., (011)/(110) peak near 18° for the Bi-rich sample and (211)/(112) peak near 40° for the V-rich sample) as compared to the stoichiometric film, suggesting that some growth orientations might be suppressed by additional Bi or V incorporation.

Raman spectra of V-rich, Bi-rich, and stoichiometric sputtered thin films are shown in Figure 4. All films have

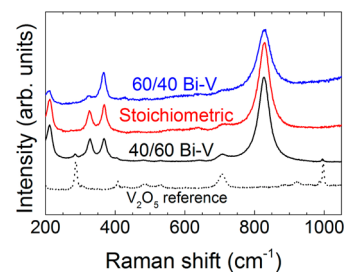


Figure 4. Micro-Raman spectra of Bi-rich (blue), V-rich (red), and stoichiometric (black) sputtered films. The spectrum of V_2O_5 reference material is also shown (dotted line).

main peaks at around 212, 327, 368, 640, 710, and 828 cm^{-1} , corresponding to the Raman active vibrational modes of monoclinic BiVO_4 .^{12,15,28,29} The spectrum from stoichiometric BiVO_4 includes only these spectral contributions and is consistent with a pure monoclinic phase film. For the Bi-rich film, the characteristic BiVO_4 Raman features decrease in intensity and become broader. We did not detect the additional bands expected for either the Raman mode of the α -phase Bi_2O_3 material (306 cm^{-1}) or the ferroelectric $\text{Bi}_2\text{VO}_{5.5}$ (850 cm^{-1}), as have been reported previously for strongly off-stoichiometric films.³⁰ For the V-rich film, we observe additional weak but sharp lines at 400 and 980 cm^{-1} , which become even more intense in films with lower Bi/V ratios. These peaks match the frequencies of the Raman-active vibrational modes of V_2O_5 and are consistent with the wire-like features in Figure 2b. In summary, while there is no evidence of phase segregation in the stoichiometric films, we observe $\text{Bi}_2\text{VO}_{5.5}$ and V_2O_5 impurity phases in the Bi-rich and V-rich films.

The surface chemical compositions of sputtered BVO thin films were investigated using XPS. As shown in Figure 5, XPS survey spectra confirm the presence of the elemental constituents, Bi, V, and O, of the deposited films. The presence of adventitious carbon allowed for calibration of the binding energy for each sample, using a standard C 1s position of 284.8 eV. No significant contribution from Sn of the underlying ITO film was observed, indicating that all films are continuous,

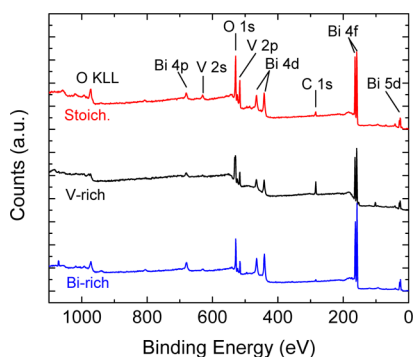


Figure 5. Survey scan X-ray photoelectron spectra from sputtered BVO thin films with different compositions: Bi-rich (blue), V-rich (black), and nearly stoichiometric (red). The elemental components of the films, Bi, V, and O, along with adventitious C, are observed for all samples.

which is consistent with morphological characterization by SEM (Figure 2).

Figure 6a and b shows spectra obtained from the Bi 4f and V 2p core level regions. The Bi 4f region is characterized by the

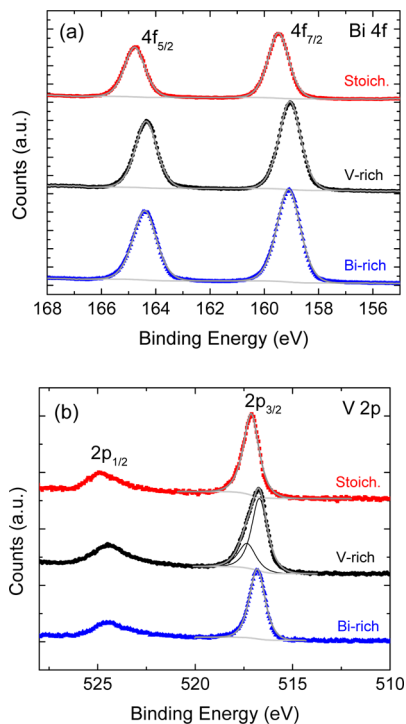


Figure 6. Narrow scan X-ray photoelectron spectra in the Bi 4f (a) and V 2p (b) core level regions from sputtered BVO thin films with different compositions: Bi-rich (blue triangles), V-rich (black circles), and nearly stoichiometric (red squares). Solid gray lines show the Shirley background and envelope fits. The thin solid lines in b show the component fits, with the high and low binding energy components assigned to V^{5+} in V_2O_5 and in $BiVO_4$, respectively.

presence of $4f_{7/2}$ and $4f_{5/2}$ components with a spin–orbit splitting of 5.3 eV and the expected branching ratio of 1.0:0.75. Likewise, the V 2p region includes $2p_{3/2}$ and $2p_{1/2}$ components with a spin orbit splitting of ~ 7.6 eV. Calculation of the surface atomic composition of each sample was performed using the total V $2p_{3/2}$ and Bi $4f_{7/2}$ spectral intensities, weighted by the corresponding atomic sensitivity factors, and yielded Bi/V

ratios of 1.9, 0.79, and 0.95 for the Bi-rich, V-rich, and stoichiometric films, respectively. The values for the V-rich and stoichiometric samples are in good agreement with the bulk compositions determined by EDS. However, XPS suggests that samples grown under Bi-rich conditions are characterized by enrichment of Bi at the surface relative to the bulk. Because Bi is more volatile than V, it is possible that excess Bi could migrate to the surface during the postannealing process and either segregate there or evaporate after migration but recondense upon cooling.

In addition to atomic composition, important information about the chemical states of the elemental constituents can be determined from XPS. Fitting of the Bi 4f spectra demonstrates that each of the spin–orbit split peaks in Figure 6a can be described by a single component, revealing that Bi is present in a single oxidation state for each sample. For all films, the binding energy position allows assignment to Bi^{3+} , with no observed contribution from Bi^{4+} .³¹ However, the binding energy position is also observed to shift as a function of composition, with Bi $4f_{7/2}$ binding energies of 159.1, 159.0, and 159.5 eV for Bi-rich, V-rich, and stoichiometric thin films, respectively. Similar composition-dependent binding energy shifts are observed in the V 2p region (*vide infra*). Therefore, it is possible to conclude that these shifts are of electronic, rather than chemical, origin. Since core level binding energies are measured relative to the Fermi level position within a material, the spectral position is inherently dependent on the doping type and concentration, with larger core level binding energies for n-type, compared to p-type, material. In the present case, the stoichiometric film is characterized by the largest binding energy, indicating that the Fermi level at the surface of this material is closer to the conduction band than for the off-stoichiometric films. We note that the Fermi level position relative to the band edges at the surface can differ from the bulk position due to the presence of a space charge region below the surface of the material. Therefore, XPS results typically provide a lower bound on the differences of the bulk Fermi level positions within the deposited films.

While analysis of the Bi 4f region reveals that Bi exists in a single chemical environment within each film, the V $2p_{3/2}$ peak for the V-rich sample (Figure 6b) includes two spectral components at 517.3 and 516.7 eV, which can be assigned to V^{5+} in V_2O_5 and V^{5+} in $BiVO_4$, respectively.³¹ The presence of two spectral components indicates phase segregation within the V-rich film and is consistent with the results from Raman spectroscopy, as well as theoretical predictions for the Bi–V–O ternary phase diagram.³² Comparison of the areal contributions of these two phases reveals that the ratio of V^{5+} in V_2O_5 to V^{5+} in $BiVO_4$ is approximately 0.3. This is in excellent agreement with the average atomic composition of the film determined via XPS, which indicated a Bi/V ratio of 0.79 (or V/Bi ratio of 1.27), and suggests phase segregation to nearly stoichiometric $BiVO_4$, with excess V present as V_2O_5 . The binding energies for V^{5+} within the Bi-rich, V-rich, and stoichiometric films of 516.8 eV, 516.7, and 517.1 eV are consistent with the differences observed between the Bi 4f peaks arising from differences of Fermi level positions for films of different compositions. While no phase segregation is observed for either the Bi-rich or stoichiometric films, the chemical shift between $BiVO_4$ and $Bi_2VO_{5.5}$ phases is, to the best of our knowledge, not known, which prevents direct assessment of the homogeneity of Bi-rich films via XPS without a phase-pure reference sample.

The photoelectrochemical (PEC) performance of the films is summarized in Figure 7. Under anodic bias, both off-

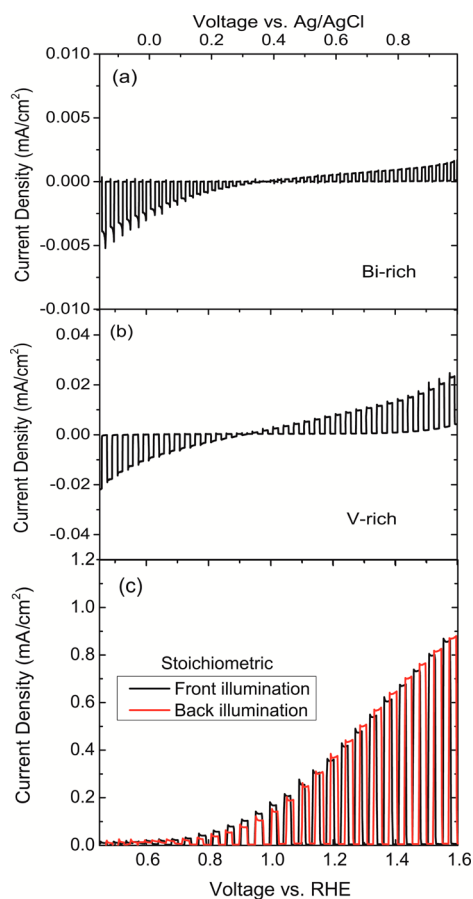


Figure 7. J – V (current density vs voltage) curves from the Bi-rich (a), V-rich (b), and stoichiometric (c) films under chopped AM 1.5 illumination (1 sun, 100 mW cm^{-2}) in pH 7 0.5 M Na_2SO_4 in 0.1 M K_2HPO_4 buffer solution. The curves from the off-stoichiometric films are the photocurrents arising from front illumination. For the stoichiometric thin film, a comparison between front and back illumination reveals identical photocurrent responses.

stoichiometric films exhibited very low photocurrent densities (Figure 7a and b). For bias $< 1 \text{ V}$ vs RHE, there is crossover to a small cathodic current. The conduction band of BiVO_4 is lower than the H_2 evolution potential,^{6,33} so this current is not due to water reduction involving BiVO_4 . We tentatively assign this phenomenon to an oxygen reduction reaction.³⁴ In contrast, the stoichiometric BiVO_4 thin film, which possesses a slight excess of V, exhibits a large and dominant photoanodic current density, with little photocathodic current at negative biases. Indeed, the photocurrent density at OER, 0.5 mA cm^{-2} , is among the best reported in the literature for unmodified BiVO_4 , and the onset potential of approximately 0.4 V vs RHE is similar to that reported for BiVO_4 thin films deposited via solution-based methods.^{7,8}

The XPS results give insight into the photoelectrochemical response of the films. The stoichiometric BiVO_4 film possesses the largest V and B core level binding energies, indicating that the surface Fermi level lies closer to the conduction band than for the off-stoichiometric films. The n-type PEC response shown in Figure 7c is consistent with this picture. By contrast, the surface Fermi level lies further from the conduction band in

both the Bi- and V-rich films. This could be indicative of both n- and p-type regions in the film, possibly due to phase segregation, which would be consistent with the ambipolar photocurrent response.

The conductivity type differences observed between the off-stoichiometric and stoichiometric films partially agree with the defect formation energy calculations published by Yin et al.³² While they found that the most influential intrinsic defects on carrier conductivity are oxygen-related defects, the oxygen content in sputtered bismuth vanadate is not studied in the present work. However, their work also pointed out that defects such as V interstitials and V substitution on Bi sites can serve as donors, a situation consistent with our highest performing stoichiometric film with a slight V enrichment. Likewise, defects such as Bi vacancies, V vacancies, and Bi substitution on V sites can serve as acceptors and result in p-type doping, which may occur for these off-stoichiometric films. Furthermore, it is possible that Bi- or V-enrichment may lead to induced defects that serve as hole-trapping sites. As a consequence, photoexcited holes can only be only extracted under high bias. The presence of such trapping sites would explain the observed p-type photocathodic current at lower bias as well as the overall poor PEC performance.

In addition to the relationship between stoichiometry and PEC performance from sputtered BiVO_4 films, we also explored differences between front illumination and back illumination. A variety of reports on solution-deposited BiVO_4 thin films have found superior photoelectrochemical performance when the material is illuminated from the back.^{7,8,15} This observation has been attributed to poor majority (electron) carrier transport in bulk BiVO_4 , which is mitigated under back illumination because the transport length from region of most intense photoexcitation is minimized. In contrast, we did not observe a significant difference of photocurrent response between back and front illumination for the case of the 100 nm thick stoichiometric film, as shown by the J – V curve in Figure 7c.

However, this observation does not necessarily imply that majority carrier (electrons) transport is significantly improved in sputtered BiVO_4 films. In fact, after sputter deposition of uniform and dense films of 100 nm thicknesses, the material remained highly insulating. When we conducted J – V measurements on a thicker film (200 nm) with the same stoichiometry, we observed a larger photocurrent density under back illumination relative to front illumination, as shown in Figure 8. However, the overall photoactivity was worse than that for the 100 nm thin film. In addition, we tested thicker films (not shown) and observed reduced photocurrent densities with distinctive, though not necessarily larger, differences between front and back illumination for increasingly thick films. For the thickest films of approximately 500–600 nm, only very tiny photocurrents were generated from both front and back side illumination.

While the enhanced photocurrent density for back illumination is clearly thickness dependent, we find that it is not entirely a consequence of poor electron transport. Rather, it is likely that the observed phenomenon is due to a combined effect from both electron and hole transport. At 100 nm, the thickness for the thin sputtered film may be close to or slightly less than the hole diffusion length in the material. In this circumstance, the holes can readily diffuse toward the surface under either front or back illumination. In this thickness regime, the hole mobility, rather than the electron mobility, dominates the charge extraction efficiency. However, when the

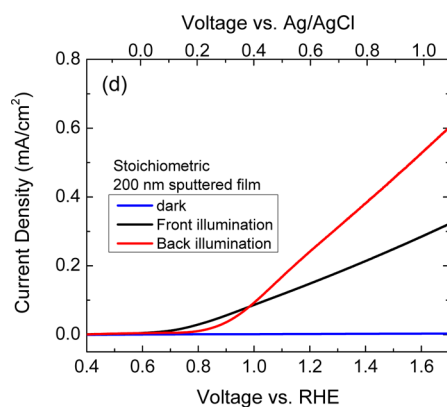


Figure 8. Comparison between J - V curves from a thicker stoichiometric sample (200 nm) under front and back illumination reveals higher photocurrent densities when the sample is illuminated from the back.

film thickness exceeds the hole diffusion length, holes generated deeper in the film may be trapped or recombine with majority electrons. Thus, in spite of increased photo absorption in thicker films, only the volume of film within the minority carrier diffusion length to the space charge region near the surface contributes to the photocurrent, and electron transport to the ITO contact becomes the limiting factor in the photocurrent density. When the sample is back illuminated, there is a shorter diffusion length for the electrons to reach the contact compared to the case for front illumination. Therefore, the charge extraction efficiency is improved compared to the front illumination, and problems associated with carrier recombination in the bulk are ameliorated. Although the overall photocurrent densities decrease under both front and back illumination due to poor electron transport and inefficient charge separation, the photocurrent density under back illumination suffers less. However, as the film thickness increases, the efficiency of charge migration of both the majority carriers to the contact and minority carriers to the surface is reduced. For the thickest films, neither front nor back illumination is effective, and only negligible photocurrents are generated. Since previously published thin film synthesis methods for BiVO_4 were primarily solution based and tended to create more porous morphologies compared to sputtering, the film thickness dependence on PEC performance in those materials was not as closely correlated with the hole diffusion length.

As implied in the previous paragraph, efficient charge carrier separation within the semiconductor is of critical importance for PEC applications. One effective method of reducing carrier recombination, and thus enhancing separation efficiency, is to add a hole-blocking layer, which prevents holes from migrating to the back contact and recombining with the electrons at the electrical contact. It has been established that metal oxides such as WO_3 ^{31,35,36} and SnO_2 ^{19,35} possess band edge energies that are suitably aligned with those of BiVO_4 for facilitating electron transport but hindering hole transport to the back contact, thus promoting directional hole transport to the electrolyte. Therefore, we investigated the effect of a hole-blocking layer on the photoelectrochemical performance of sputtered stoichiometric BiVO_4 thin films by adding a WO_3 layer underneath the BiVO_4 . A 100 nm thick WO_3 film was first deposited by reactive sputtering on ITO-coated glass. Then, a stoichiometric (slightly enriched in V) 100 nm BiVO_4 thin film

was reactively sputtered on top of the WO_3 film. Figure 9 shows a comparison of J - V curves from BiVO_4 with and

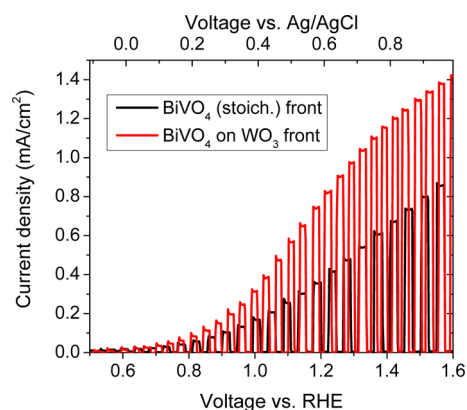


Figure 9. J - V (current density vs voltage) curves of BiVO_4 thin films with and without a WO_3 hole-blocking layer. The samples were tested in a three electrode configuration under front side chopped illumination with an AM1.5, 100 W/cm^2 light source and in pH 7 buffer solution.

without a WO_3 hole-blocking layer under chopped front side illumination. Strikingly, an improvement of the photocurrent density by nearly a factor of 2 at 1.2 V vs RHE can be achieved by the addition of the WO_3 underlayer. Furthermore, in the case of the BiVO_4 thin film with a WO_3 underlayer, PEC measurements reveal that front illumination yields larger photocurrent densities than back illumination.

We considered the possibility that the WO_3 layer might contribute to the photocurrent. The PEC performance of the WO_3 layer by itself is shown in Figure S1 (Supporting Information); the observed photocurrent is more than an order of magnitude smaller than that of the double layer structure. We also compare in Figure S3 (Supporting Information) the transmission spectra of a 100 nm BiVO_4 film and a 100 nm BiVO_4 /100 nm WO_3 structure. The transmission spectra are nearly identical; in the double layer structure, most of the light is absorbed in the BiVO_4 layer.

Figure 10 displays the IPCE of the BiVO_4 thin film with a WO_3 underlayer, a result in close agreement with the inset

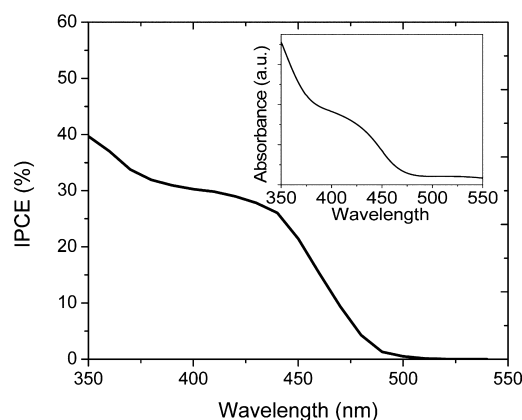


Figure 10. IPCE spectrum of a BiVO_4 thin film with a 100 nm thick WO_3 hole-blocking layer on an ITO substrate with an inset of optical absorption spectrum of the film. The sample was held at 1.2 V versus RHE in a three electrode configuration and was illuminated from the front side in pH 7 buffer solution.

absorbance spectrum of the film measured. The IPCE exhibits a photocurrent onset near 490 nm, which rises steeply to IPCE values of 30% to 40% at wavelengths shorter than ~ 450 nm. The steep IPCE decrease at wavelengths larger than 440–450 nm is consistent with previous reports^{7,17,19} and is a consequence of above-bandgap optical absorption. However, the small tail of IPCE and absorption response out to ~ 500 nm is due to weak light absorption at the band edge, which may suggest that BiVO₄ possesses an indirect bandgap that is slightly narrower than its direct transition¹⁹ or that band edge tail states induced by regions of disorder contribute to the photoelectrochemical response. Figure S4 (Supporting Information) shows Tauc plots of BiVO₄ films which are consistent with this picture.

IV. CONCLUSIONS

We synthesized high quality BiVO₄ thin films by reactive cosputtering for the first time and explored the influence of the Bi/V ratio on structure, morphology, and PEC performances. For Bi-rich and V-rich films, they showed some degree of phase separation and both weak photoanodic and photocathodic current responses. Near-stoichiometric BiVO₄ (with slight V rich) showed a photocathodic response with a much higher current density. We also discussed the influence of front illumination versus back illumination, finding that the influence of illumination side was film thickness dependent and might be a combined effect from both electron and hole transport. In addition, we improved carrier separation by adding a WO₃ hole-blocking layer. In the future, we will work on the further improvement of BiVO₄ thin films for PEC application such as improving the conductivity by doping and loading OER catalysts, as well as using high quality sputtered BiVO₄ thin films as platforms for fundamental studies of this material.

■ ASSOCIATED CONTENT

Supporting Information

Photoelectrochemical testing of sputtered WO₃ photoanodes; photoelectrochemical stability of BiVO₄/WO₃ photoanodes; optical characterization of BiVO₄ and BiVO₄/WO₃ photoanodes; cross-sectional SEM image of BiVO₄/WO₃ layers on ITO coated glass substrate. This material is available free of charge via the Internet at <http://pubs.acs.org>.

■ AUTHOR INFORMATION

Corresponding Author

*Joint Center for Artificial Photosynthesis, Lawrence Berkeley National Laboratory, MS62R0203, 1 Cyclotron Road, Berkeley, CA 94720. Phone: 1-510-486-6715. Fax: 1-510-486-4995. E-mail: JWAger@lbl.gov.

Notes

The authors declare no competing financial interest.

■ ACKNOWLEDGMENTS

This material is based upon work performed by the Joint Center for Artificial Photosynthesis, a DOE Energy Innovation Hub, supported through the Office of Science of the U.S. Department of Energy under Award Number DE-SC0004993. E.A.L. also acknowledges fellowship support from Marie Curie Actions Program.

■ ABBREVIATIONS

PEC, photoelectrochemical; RHE, reversible hydrogen electrode; $J-V$, current–voltage; J_{SC} , short-circuit current; IPCE, incident photon to charge conversion efficiency; SEM, scanning electron microscope; XRD, X-ray diffraction

■ REFERENCES

- (1) Kudo, A.; Ueda, K.; Kato, H.; Mikami, I. Photocatalytic O₂ Evolution under Visible Light Irradiation on BiVO₄ in Aqueous AgNO₃ Solution. *Catal. Lett.* **1998**, *53*, 229–230.
- (2) Sayama, K.; Nomura, A.; Arai, T.; Sugita, T.; Abe, R.; Yanagida, M.; Oi, T.; Iwasaki, Y.; Abe, Y.; Sugihara, H. Photoelectrochemical Decomposition of Water into H₂ and O₂ on Porous BiVO₄ Thin-Film Electrodes under Visible Light and Significant Effect of Ag Ion Treatment. *J. Phys. Chem. B* **2006**, *110*, 11352–11360.
- (3) Long, M.; Cai, W. M.; Cai, J.; Zhou, B. X.; Chai, X. Y.; Wu, Y. H. Efficient Photocatalytic Degradation of Phenol over Co₃O₄/BiVO₄ Composite under Visible Light Irradiation. *J. Phys. Chem. B* **2006**, *110*, 20211–20216.
- (4) Kohtani, S.; Koshiko, M.; Kudo, A.; Tokumura, K.; Ishigaki, Y.; Toriba, A.; Hayakawa, K.; Nakagaki, R. Photodegradation of 4-alkylphenols Using BiVO₄ Photocatalyst under Irradiation with Visible Light from A Solar Simulator. *Appl. Catal., B* **2003**, *46*, 573–586.
- (5) Kudo, A.; Miseki, Y. Heterogeneous Photocatalyst Materials for Water Splitting. *Chem. Soc. Rev.* **2009**, *38*, 253–278.
- (6) Park, Y.; McDonald, K. J.; Choi, K. S. Progress in Bismuth Vanadate Photoanodes for Use in Solar Water Oxidation. *Chem. Soc. Rev.* **2013**, *42*, 2321–2337.
- (7) Abdi, F. F.; van de Krol, R. Nature and Light Dependence of Bulk Recombination in Co-Pi-Catalyzed BiVO₄ Photoanodes. *J. Phys. Chem. C* **2012**, *116*, 9398–9404.
- (8) Luo, W. J.; Yang, Z. S.; Li, Z. S.; Zhang, J. Y.; Liu, J. G.; Zhao, Z. Y.; Wang, Z. Q.; Yan, S. C.; Yu, T.; Zou, Z. G. Solar Hydrogen Generation from Seawater with A Modified BiVO₄ Photoanode. *Energy Environ. Sci.* **2011**, *4*, 4046–4051.
- (9) Tong, L.; Iwase, A.; Nattestad, A.; Bach, U.; Weidener, M.; Gotz, G.; Mishra, A.; Bauerle, P.; Amal, R.; Wallace, G. G.; et al. Sustained Solar Hydrogen Generation Using a Dye-Sensitized NiO Photocathode/BiVO₄ Tandem Photo-electrochemical Device. *Energy Environ. Sci.* **2012**, *5*, 9472–9475.
- (10) Zhang, L.; Chen, D. R.; Jiao, X. L. Monoclinic Structured BiVO₄ Nanosheets: Hydrothermal Preparation, Formation Mechanism, and Coloristic and Photocatalytic Properties. *J. Phys. Chem. B* **2006**, *110*, 2668–2673.
- (11) Zhou, L.; Wang, W. Z.; Zhang, L.; Xu, H. L.; Zhu, W. Single-crystalline BiVO₄ Microtubes with Square Cross-sections: Microstructure, Growth Mechanism, and Photocatalytic Property. *J. Phys. Chem. C* **2007**, *111*, 13659–13664.
- (12) Kudo, A.; Omori, K.; Kato, H. A Novel Aqueous Process for Preparation of Crystal Form-Controlled and Highly Crystalline BiVO₄ Powder from Layered Vanadates at Room Temperature and Its Photocatalytic and Photophysical Properties. *J. Am. Chem. Soc.* **1999**, *121*, 11459–11467.
- (13) Abdi, F. F.; Firet, N.; van de Krol, R. Efficient BiVO₄ Thin Film Photoanodes Modified with Cobalt Phosphate Catalyst and W-doping. *ChemCatChem* **2013**, *5*, 490–496.
- (14) Li, Z. S.; Luo, W. J.; Zhang, M. L.; Feng, J. Y.; Zou, Z. G. Photoelectrochemical Cells for Solar Hydrogen Production: Current State of Promising Photoelectrodes, Methods to Improve Their Properties, and Outlook. *Energy Environ. Sci.* **2013**, *6*, 347–370.
- (15) Seabold, J. A.; Choi, K. S. Efficient and Stable Photo-Oxidation of Water by a Bismuth Vanadate Photoanode Coupled with an Iron Oxyhydroxide Oxygen Evolution Catalyst. *J. Am. Chem. Soc.* **2012**, *134*, 2186–2192.
- (16) Ding, C. M.; Shi, J. Y.; Wang, D. G.; Wang, Z. J.; Wang, N.; Liu, G. J.; Xiong, F. Q.; Li, C. Visible Light Driven overall Water Splitting Using Cocatalyst/BiVO₄ Photoanode with Minimized Bias. *Phys. Chem. Chem. Phys.* **2013**, *15*, 4589–4595.

- (17) Berglund, S. P.; Flaherty, D. W.; Hahn, N. T.; Bard, A. J.; Mullins, C. B. Photoelectrochemical Oxidation of Water Using Nanostructured BiVO₄ Films. *J. Phys. Chem. C* **2011**, *115*, 3794–3802.
- (18) Jia, Q. X.; Iwashina, K.; Kudo, A. Facile Fabrication of An Efficient BiVO₄ Thin Film Electrode for Water Splitting under Visible Light Irradiation. *Proc. Natl. Acad. Sci. U.S.A.* **2012**, *109*, 11564–11569.
- (19) Liang, Y. Q.; Tsubota, T.; Mooij, L. P. A.; van de Krol, R. Highly Improved Quantum Efficiencies for Thin Film BiVO₄ Photoanodes. *J. Phys. Chem. C* **2011**, *115*, 17594–17598.
- (20) Saito, R.; Miseki, Y.; Sayama, K. Highly Efficient Photoelectrochemical Water Splitting Using a Thin Film Photoanode of BiVO₄/SnO₂/WO₃ Multi-composite in A Carbonate Electrolyte. *Chem. Commun.* **2012**, *48*, 3833–3835.
- (21) Berglund, S. P.; Rettie, A. J. E.; Hoang, S.; Mullins, C. B. Incorporation of Mo and W into Nanostructured BiVO₄ Films for Efficient Photoelectrochemical Water Oxidation. *Phys. Chem. Chem. Phys.* **2012**, *14*, 7065–7075.
- (22) Chen, L.; Graham, M. E.; Li, G. H.; Gray, K. A. Fabricating Highly Active Mixed Phase TiO₂ Photocatalysts by Reactive DC Magnetron Sputter Deposition. *Thin Solid Films* **2006**, *515*, 1176–1181.
- (23) Di Franco, F.; Santamaria, M.; Di Quarto, F.; Tsuji, E.; Habazaki, H. The Influence of Nitrogen Incorporation on the Optical Properties of Anodic Ta₂O₅. *Electrochim. Acta* **2012**, *59*, 382–386.
- (24) Marsen, B.; Miller, E. L.; Paluselli, D.; Rocheleau, R. E. Progress in Sputtered Tungsten Trioxide for Photoelectrode Applications. *Int. J. Hydrogen. Energy* **2007**, *32*, 3110–3115.
- (25) Fedorov, V. I.; Davydov, I. Y. Thermoelectric Properties of Vanadium, Bismuth, and Antimony Oxides in the Temperature Interval 500–1500 Degree-K. *High Temp.* **1978**, *16*, 654–660.
- (26) Chen, Z. B.; Jaramillo, T. F.; Deutsch, T. G.; Kleiman-Shwarsstein, A.; Forman, A. J.; Gaillard, N.; Garland, R.; Takanabe, K.; Heske, C.; Sunkara, M.; et al. Accelerating Materials Development for Photoelectrochemical Hydrogen Production: Standards for Methods, Definitions, and Reporting Protocols. *J. Mater. Res.* **2010**, *25*, 3–16.
- (27) Tokunaga, S.; Kato, H.; Kudo, A. Selective Preparation of Monoclinic and Tetragonal BiVO₄ with Scheelite Structure and Their Photocatalytic Properties. *Chem. Mater.* **2001**, *13*, 4624–4628.
- (28) Yu, J. Q.; Kudo, A. Effects of Structural Variation on the Photocatalytic Performance of Hydrothermally Synthesized BiVO₄. *Adv. Funct. Mater.* **2006**, *16*, 2163–2169.
- (29) Dall'Antonia, L. H.; de Tacconi, N. R.; Chanmanee, W.; Timmaji, H.; Myung, N.; Rajeshwar, K. Electrosynthesis of Bismuth Vanadate Photoelectrodes. *Electrochem. Solid State Lett.* **2010**, *13*, D29–D32.
- (30) Barreca, D.; Depero, L. E.; Di Noto, V.; Rizzi, G. A.; Sangaletti, L.; Tondello, E. Thin Films of Bismuth Vanadates with Modifiable Conduction Properties. *Chem. Mater.* **1999**, *11*, 255–261.
- (31) Su, J.; Zou, X. X.; Li, G. D.; Wei, X.; Yan, C.; Wang, Y. N.; Zhao, J.; Zhou, L. J.; Chen, J. S. Macroporous V₂O₅-BiVO₄ Composites: Effect of Heterojunction on the Behavior of Photogenerated Charges. *J. Phys. Chem. C* **2011**, *115*, 8064–8071.
- (32) Yin, W. J.; Wei, S. H.; Al-Jassim, M. M.; Turner, J.; Yan, Y. F. Doping Properties of Monoclinic BiVO₄ Studied by First-Principles Density-Functional Theory. *Phys. Rev. B* **2011**, *83*.
- (33) Chen, S. Y.; Wang, L. W. Thermodynamic Oxidation and Reduction Potentials of Photocatalytic Semiconductors in Aqueous Solution. *Chem. Mater.* **2012**, *24*, 3659–3666.
- (34) Lin, Y. J.; Xu, Y.; Mayer, M. T.; Simpson, Z. I.; McMahon, G.; Zhou, S.; Wang, D. W. Growth of p-Type Hematite by Atomic Layer Deposition and Its Utilization for Improved Solar Water Splitting. *J. Am. Chem. Soc.* **2012**, *134*, 5508–5511.
- (35) Chatchai, P.; Murakami, Y.; Kishioka, S. Y.; Nosaka, A. Y.; Nosaka, Y. FTO/SnO₂/BiVO₄ Composite Photoelectrode for Water Oxidation under Visible Light Irradiation. *Electrochem. Solid State Lett.* **2008**, *11*, H160–H163.
- (36) Hong, S. J.; Lee, S.; Jang, J. S.; Lee, J. S. Heterojunction BiVO₄/WO₃ Electrodes for Enhanced Photoactivity of Water Oxidation. *Energy Environ. Sci.* **2011**, *4*, 1781–1787.